Modeling of Reverse Osmosis in the Presence of Strong Solute-Membrane Affinity

H. Mehdizadeh and J. M. Dickson
Dept. of Chemical Engineering, McMaster University, Hamilton, Ontario, Canada L8S 4L7

Modeling of reverse osmosis in the presence of strong solute-membrane affinity has always been a challenge due to the complexity of the solute-solvent-membrane interactions and the resultant effect on membrane performance. Most transport models, including all models treating membranes as nonporous and those based on irreversible thermodynamics, are unable to describe or to predict all of the phenomena associated with this case. Recently, the modified surface force-pore flow model has been derived and used to describe the performance of reverse osmosis membranes for solutes which are rejected from the membrane. In the present work, this model is extended to a more general form which can describe the solute-membrane affinity case. For illustration, the extended model, with five adjustable parameters, is used to describe the performance for cellulose acetate membranes and dilute aqueous solutions of toluene, cumene, and p-chlorophenol (data from literature). The model is reasonably consistent with the data. Simulation results of the extended model are also shown.

Introduction

It is well known that the reverse osmosis performance for certain low molecular weight organics in water, such as toluene, benzene, and phenol derivatives, is markedly different than those for simple aqueous salt solutions (Lonsdale et al., 1967; Matsuura and Sourirajan, 1973a,b; Anderson et al., 1972; Burghoff et al., 1980; Lloyd et al., 1982). This anomalous behavior is associated with a strong affinity between the organic solute and the membrane material such that the uncharged organic molecules are sorbed into the membrane rather than the usual case, in reverse osmosis, of being rejected by the membrane. The nature of this affinity is due to nonpolar or polar interactions in a system. For example, strong nonpolar attraction exists between a nonpolar hydrocarbon solute and the (nonpolar) backbone of the cellulose acetate polymer, and strong polar attraction exists between a solute such as phenol and the polar functionality of the cellulose acetate material, which is stronger than the water-membrane attraction. For inorganic molecules and many organic molecules the water-membrane affinity dominates and the more common mechanism of reverse osmosis solute rejection is observed.

The characteristic behavior for a strong solute-membrane affinity system can be summarized by the following: increasing the operating pressure decreases the separation; permeate flux is usually much less than pure water flux even when osmotic effects are small; partition coefficients are larger than unity; and separation can be positive, zero, or negative, depending on specific operating conditions (Matsuura and Sourirajan, 1971; Matsuura et al., 1974; Dickson et al., 1979; Dickson et al., 1983; Dickson, 1985; Connell and Dickson, 1988). Typical concentration behaviors are shown in Figure 1 (Mehdizadeh and Dickson, 1989b; Mehdizadeh, 1990). Figures 1a and 1b represent typical profiles in a solute-membrane affinity system in contrast with the more usual case of solvent-membrane affinity shown in Figure 1c ("b.l." stands for "boundary layer"). Negative separation may happen for some systems, such as p-chlorophenol-water-cellulose acetate system, as shown in Figure 1b.

Attempts to quantitatively model cases where strong solute-membrane affinity exist have met with different degrees of success. Lonsdale et al. (1967) first noted such behavior for phenol-water separation with cellulose acetate membranes and explained the results in terms of solute-solvent coupling. However, they were not able to model the data. Since then several authors have successfully modeled the data using the finely porous model (4-parameter version) or irreversible thermo-

Correspondence concerning this article should be addressed to J. M. Dickson.

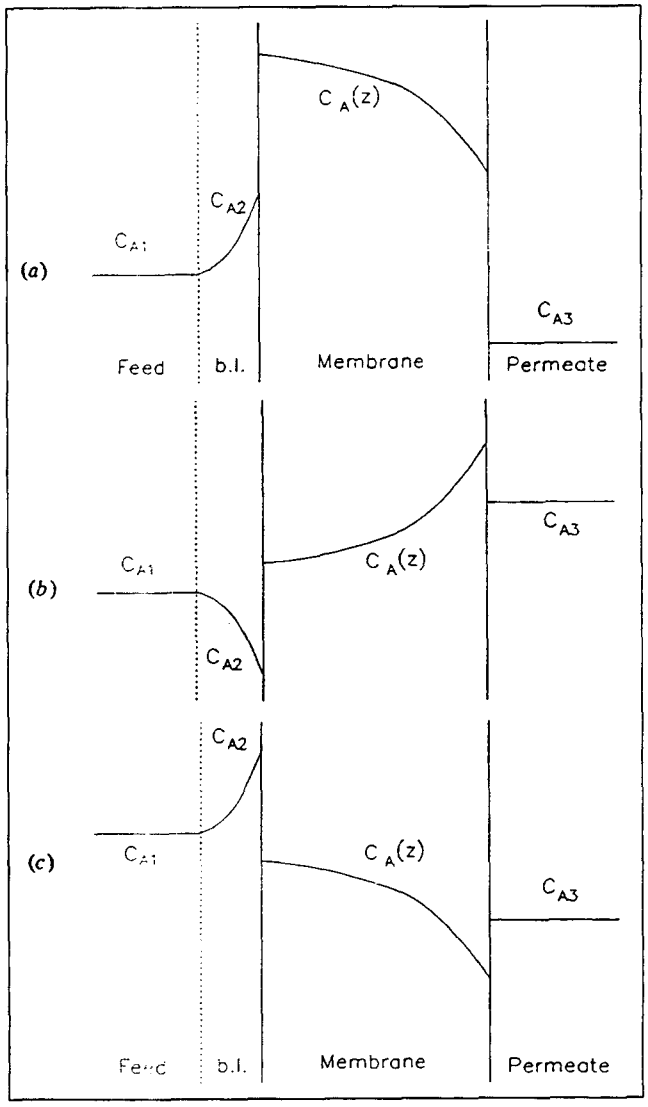

Figure 1. Concentration profile and partitioning effect in reverse osmosis.

(a) Solute-membrane affinity system with positive separation; (b) solute-membrane affinity system with negative separation; and (c) solvent-membrane affinity system (always positive separation).

dynamics-phenomenological transport relationship (Jonsson and Boesen, 1975; Jonsson, 1978; Burghoff et al., 1980). Thiel et al. (1985a,b) have explained the flux decrease using an irreversible thermodynamics approach accounting for the strengths of the solute-solvent-membrane interactions and an adsorption isotherm, but could not explain the separation behavior for these systems. In fact, none of the above have been able to predict the behavior that separation can decrease from positive to negative separation with increasing volume flux as is observed for solutes such as p-chlorophenol (Dickson et al., 1979; Dickson, 1985).

A recent model for reverse osmosis transport, called the Modified Surface Force-Pore Flow (MD-SF-PF) model (Mehdizadeh and Dickson, 1989a), which reformulates and corrects the Surface Force-Pore Flow (SF-PF) model (Matsuura and Sourirajan, 1981), has been used successfully to describe and

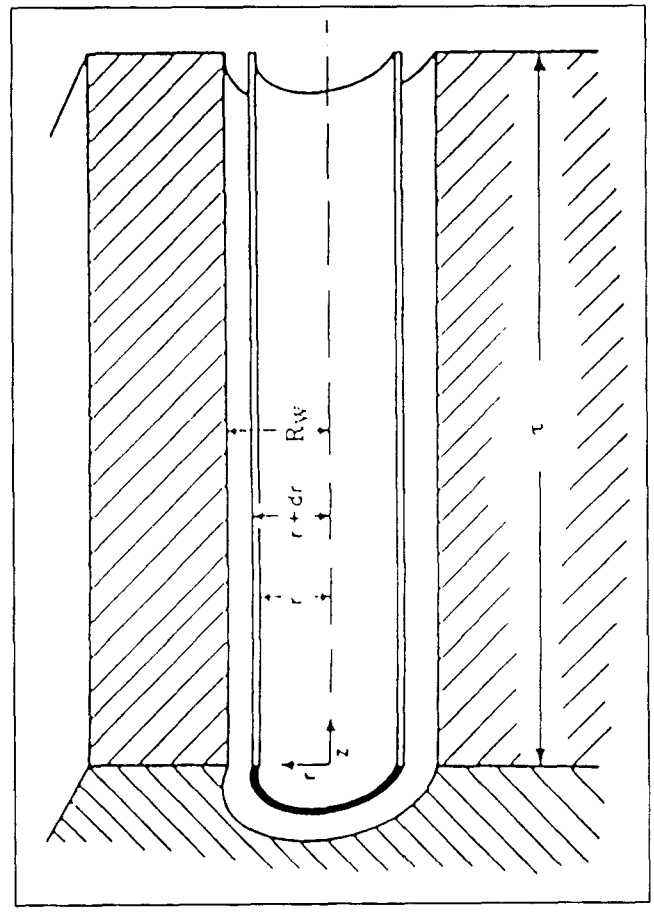

Figure 2. Cylindrical coordinate system in a membrane pore.

predict the usual phenomenon of solute exclusion from reverse osmosis membrane (Mehdizadeh and Dickson, 1989b and 1991).

The MD-SF-PF model assumes the membrane to be microporous and models the pores as perfect right cylinders. A two-dimensional approach is used (see Figure 2) in which the solute velocity and concentration in the pore vary in both radial, r, and axial, z, directions. A balance of applied and frictional forces acting on the solute in the pore is given as a function of the radial and axial positions. The solute-membrane interactions are expressed by a Sutherland-type potential function. A friction parameter, b, which is the ratio of solute diffusivity in free solution to solute diffusivity inside a pore, is used to describe the hydrodynamic drag on the solute by the pore wall. Continuum mechanics are assumed to be valid (see, for example, Mehdizadeh and Dickson, 1991; Jacazio et al., 1972).

In the present article, the MD-SF-PF model is extended to a more general form to describe the complex behavior of solute-membrane affinity systems. Derivation of the extended model is given in the Theory Section. The model, called the Extended MD-SF-PF model, hereafter, is compared to literature data for three solutes, and simulation results are presented.

Theory

The Extended MD-SF-PF model differs in the following

three aspects from the original MD-SF-PF model:

- The chemical potential of solute takes into account the effect of the pressure-induced solute transport. This additional term may be important for solutes with high partial molar volumes and membranes that have relatively low solute-water separation.
- The membrane surface potential function is assumed to be concentration dependent so that the surface potential varies as a function of both radial and axial positions inside the membrane. In the original MD-SF-PF model, the potential function varies only with radial direction, so that the partition coefficients on the high- and low-pressure sides of the membrane become equal. However, the partition coefficient may vary with concentration, membrane structure, temperature, and possibly pressure. In this work, a model for the variation of the potential function with radial and axial positions, inside the membrane, is proposed; as a result, the partition coefficients at the ends of the membrane may be different.
- The hydrodynamic friction function between the solute and the membrane, b, is assumed to vary in the radial direction inside the membrane pores. In the original MD-SF-PF model, this function is given by the Faxen equation which assumes the friction function is constant (that is, independent of radial position).

In this section, the extended MD-SF-PF model is derived in a manner paralleling the MD-SF-PF model (Mehdizadeh and Dickson, 1989a). First, the radial component of the solute flux and then the axial component of the solute flux together with the equation of continuity are examined. Finally, the equations required to describe the overall flux and separation are presented.

Radial component of solute flux

Following the assumption of radial equilibrium (Anderson and Malone, 1974), the radial component of the solute flux in a pore is:

$$\frac{J_{A,r}}{-D_{AB}}=\frac{\partial C_A(r,z)}{\partial r}+\frac{C_A(r,z)}{RT}\frac{\partial \phi(r,z)}{\partial r}=0 \tag{1}$$

where the pore wall potential, $\phi(r, z)$, which is the net body force acting on the solute by the pore wall, can be positive (indicating the solute is repelled by the pore wall) or negative (indicating the solute is attracted by the pore wall). Integration of Eq. 1 leads to the following Boltzmann equations at the pore entrance:

$$C_A(r,0)=C_{A2}\exp\left[-\frac{\phi(r,0)}{RT}\right] \tag{2}$$

and similarly at the pore exit:

$$C_A(r,\tau)=C_{A3}\exp\left[-\frac{\phi(r,\tau)}{RT}\right] \tag{3}$$

Derivation of Eqs. 2 and 3 closely parallels that in Appendix A previously (Mehdizadeh and Dickson, 1989a) and is used by others (for example, Anderson and Malone, 1974).

The above results, Eqs. 2 and 3, can also be interpreted in terms of the radial dependent partition coefficients on the high- and low-pressure sides of the membrane:

$$K_2(\rho)=\frac{C_A(\rho,\xi=0)}{C_{A2}}=\exp\left[-\frac{\phi(r,0)}{RT}\right]=\exp[-\Phi(\rho,0)] \tag{4}$$

$$K_3(\rho)=\frac{C_A(\rho,\xi=1)}{C_{A3}}=\exp\left[-\frac{\phi(r,\tau)}{RT}\right]=\exp[-\Phi(\rho,1)] \tag{5}$$

written in terms of the dimensionless radial, $\rho=r/R_W$, and axial $\xi=z/\tau$, positions and the dimensionless potential, $\Phi(\rho,\xi)=\phi(r, z)/RT$. The partition coefficients are different since the potential functions are different at the ends of a pore.

Averaging Eqs. 4 and 5 over the pore radius the effective (average) partition coefficients, K_2 and K_3, are obtained as:

$$K_2=\frac{\int_0^{1-\lambda}K_2(\rho)\rho d\rho}{\int_0^1\rho d\rho}=2\int_0^{1-\lambda}e^{-\Phi(\rho,0)}\rho d\rho \tag{6}$$

$$K_3=\frac{\int_0^{1-\lambda}K_3(\rho)\rho d\rho}{\int_0^1\rho d\rho}=2\int_0^{1-\lambda}e^{-\Phi(\rho,1)}\rho d\rho \tag{7}$$

where λ is the ratio of solute molecular radius to the pore radius. Knowing the potential function, $\Phi(\rho,\xi)$, one can determine the partition coefficients from Eqs. 6 and 7.

Axial component of solute flux and equation of continuity

The total driving force of solute is given by the chemical potential gradient inside the pore (Anderson and Malone, 1974),

$$F_A(r,z)=-\frac{\partial \mu_A(r,z)}{\partial z} \tag{8}$$

where the total solute potential (sum of chemical potential plus potential due to body force between solute and membrane (see, for example, Higuchi and Nakagawa (1989))) is:

$$\mu_A=\mu_A^0+RT\ln a_A+v_AP+\phi(r,z) \tag{9}$$

The v_AP term is included in Eq. 9 ultimately to account for the transport of solute molecules by pressure forces. Assuming the solution to be ideal, the gradient can be written as:

$$\frac{\partial \mu_A(r,z)}{\partial z}=\frac{1}{C_A(r,z)}\frac{\partial[RTC_A(r,z)]}{\partial z}+v_A\frac{\partial P(r,z)}{\partial z}+\frac{\partial \phi(r,z)}{\partial z} \tag{10}$$

Since the gradient of the chemical potential is what drives the solute through the pore, then the gradient of the potential function contributes to this driving force. As discussed later

in the article, we do not know the exact form of the potential function at this point so the term is neglected in this equation. This simplification can be justified if the concentration and pressure contributions to solute flow are large compared to the potential contribution, which will be the case if ϕ does not vary strongly with concentration. Inclusion of this effect will be presented in a future article.

Equation 8, upon using van't Hoff's equation for solution osmotic pressure, becomes:

$$F_A(r,z) = -\frac{RT}{\pi(r,z)}\frac{\partial \pi(r,z)}{\partial z} - v_A\frac{\partial P(r,z)}{\partial z} \tag{11}$$

This equation is used in a force balance on solute inside the pore, as presented in Appendix I, to derive the axial component of the equation of solute flux as:

$$J_{A,z}(\rho) = \frac{1}{\tau\chi_{AB}b(\rho)}\left\{-\frac{\partial \pi(\rho,\xi)}{\partial \xi} - v_A\frac{\pi(\rho,\xi)}{RT}\frac{\partial P(\rho,\xi)}{\partial \xi} + \alpha(\rho)\pi(\rho,\xi)\right\} \tag{12}$$

where the friction coefficient χ_{AB} is defined as:

$$\chi_{AB} = -\frac{F_{AB}(\rho,\xi)}{[u_A(\rho,\xi) - u_B(\rho)]} \tag{13}$$

and $b(\rho)$ and $\alpha(\rho)$ are the friction function and fluid velocity defined as:

$$b(\rho) = \frac{\chi_{AB} + \chi_{AM}(\rho)}{\chi_{AB}} = \frac{D_{AB}}{D_{AM}(\rho)} \tag{14}$$

$$\alpha(\rho) = \frac{u_B(\rho)\tau}{D_{AB}} \tag{15}$$

The equation of continuity of solute states that:

$$\nabla \cdot J_A = 0 \tag{16}$$

which reduces to the following form for the present problem:

$$\frac{\partial J_{A,z}}{\partial \xi} = 0 \tag{17}$$

Then, combining the above equation with Eq. 12 yields the following equation:

$$\frac{\partial^2 \pi(\rho,\xi)}{\partial \xi^2} + \frac{v_A}{RT}\frac{\partial}{\partial \xi}\left\{\pi(\rho,\xi)\frac{\partial P(\rho,\xi)}{\partial \xi}\right\} - \alpha(\rho)\frac{\partial \pi(\rho,\xi)}{\partial \xi} = 0 \tag{18}$$

Assuming that (Mehdizadeh and Dickson, 1989a) pressure is linear in ξ, then:

$$\frac{\partial P(\rho,\xi)}{\partial \xi} = P(\rho,1) - P(\rho,0) \tag{19}$$

where

$$P(\rho,1) - P(\rho,0) = -\Delta P + \pi_2\sigma_2(\rho) - \pi_3\sigma_3(\rho) \tag{20}$$

and subject to the boundary conditions,

$$\pi(\rho,0) = \pi_2 e^{-\Phi(\rho,0)} \tag{21}$$

$$\pi(\rho,1) = \pi_3 e^{-\Phi(\rho,1)} \tag{22}$$

gives the profiles of osmotic pressure or concentration inside the pore,

$$\pi(\rho,\xi) = \left\{\pi_2 - [\pi_2 - K^*(\rho)\pi_3]\frac{e^{[\alpha(\rho)+\omega(\rho)]\xi} - 1}{e^{[\alpha(\rho)+\omega(\rho)]} - 1}\right\}e^{-\Phi(\rho,0)} \tag{23}$$

$$C_A(\rho,\xi) = \left\{C_{A2} - \left[C_{A2} - K^*(\rho)C_{A3}\right]\frac{e^{[\alpha(\rho)+\omega(\rho)]\xi} - 1}{e^{[\alpha(\rho)+\omega(\rho)]} - 1}\right\}e^{-\Phi(\rho,0)} \tag{24}$$

where $K^*(\rho)$ is the ratio of the radial partition coefficient at the ends of the pore,

$$K^*(\rho) = \frac{e^{-\Phi(\rho,1)}}{e^{-\Phi(\rho,0)}} \tag{25}$$

and $\omega(\rho)$ represents the solute velocity induced by pressure forces, defined as:

$$\omega(\rho) = \frac{v_A}{RT}\{\Delta P - [\sigma_2(\rho)\pi_2 - \sigma_3(\rho)\pi_3]\} \tag{26}$$

Therefore, Eq. 26, represents the solute flow as contributed by pressure forces; this solute flux is ignored in the MD-SF-PF model. The $\sigma_2(\rho)$ and $\sigma_3(\rho)$ in Eq. 26 are defined as:

$$\sigma_2(\rho) = 1 - e^{-\Phi(\rho,0)} \tag{27}$$

$$\sigma_3(\rho) = 1 - e^{-\Phi(\rho,1)} \tag{28}$$

It is interesting to note that the $\sigma_2(\rho)$ and $\sigma_3(\rho)$ are local Staverman (or reflection) coefficients at each side of the membrane. The larger the partial molar volume of the solute, v_A, and/or the higher the operating pressure, ΔP, the larger is the pressure-induced transport of the solute.

Equation 24 is very interesting; the phenomenon of solute repulsion or attraction is highly dependent on the ratio of the potential functions $K^*(\rho)$ across the membrane. That is, if the ratio $K^*(\rho)$ is such that $K^*(\rho)C_{A3}$ becomes smaller than C_{A2}, then concentration decreases along the pore length and, therefore, positive separation is calculated. On the other hand, if the potential is such that the ratio $K^*(\rho)$ is such that $K^*(\rho)C_{A3}$ becomes larger than C_{A2}, then concentration increases along the pore length and, therefore, negative separation is calculated. Some real examples of solute-membrane affinity, for both negative and positive separation systems, are presented in the Results and Discussion Section.

Of the factors that could affect the magnitude of $K^*(\rho)$, the most probable is a concentration dependence of K_i. This concentration dependence is likely caused by the strong solute-solute interaction that would exist in addition to the strong

solute-membrane interaction. Interestingly, by Eq. 24, the ratio $K^*(\rho)$ can be small or large (leading to positive or negative separation, respectively) even if K_i values are less than 1. However, care is required in using Eq. 24 alone since C_{A2} and C_{A3} must also conform to momentum and material balance on the pore fluid, as derived in the next two sections, and cannot be chosen randomly.

Finally, substituting Eqs. 23, 19, 20 and AI.8 (see Appendix I) into Eq. 12 gives an explicit expression for the solute flux,

$$J_{A,z}(\rho)=\left[\frac{\alpha(\rho)+\omega(\rho)}{\tau\chi_{AB}b(\rho)}\right]\left\{\pi_2+\frac{\pi_2-K^*(\rho)\pi_3}{e^{[\alpha(\rho)+\omega(\rho)]}-1}\right\}e^{-\Phi(\rho,0)} \quad (29)$$

This equation is used, in the following sections, to determine membrane separation and flux.

Derivation of velocity profile

A force balance in the z direction on the fluid element, in the annular region between z and $z+dz$ and between r and $r+dr$ (Figure 2), yields the differential equation for the fluid velocity profile inside the pore as shown in Appendix II. The result is:

$$\left(\frac{d^2\alpha(\rho)}{d\rho^2}+\frac{1}{\rho}\frac{d\alpha(\rho)}{d\rho}\right)+\frac{1}{\beta_1}\left\{\frac{\Delta P}{\pi_2}-\frac{\pi_2\sigma_2(\rho)-\pi_3\sigma_3(\rho)}{\pi_2}\right\}$$
$$-\frac{1}{\beta_1}\left[1-\frac{1}{b(\rho)}\right][\alpha(\rho)$$
$$+\omega(\rho)]\left\{1+\frac{1-(\pi_3/\pi_2)K^*(\rho)}{e^{[\alpha(\rho)+\omega(\rho)]}-1}\right\}e^{-\Phi(\rho,0)}=0 \quad (30)$$

where

$$\beta_1=\frac{\eta D_{AB}}{R_W^2\pi_2} \quad (31)$$

and $\alpha(\rho)$, $K^*(\rho)$, and $\omega(\rho)$ are defined by Eqs. 15, 25 and 26, respectively. The boundary conditions for the velocity profile are:

$$\alpha(\rho)=0 \quad \text{at } \rho=1 \quad (32)$$

$$\frac{d\alpha(\rho)}{d\rho}=0 \quad \text{at } \rho=0 \quad (33)$$

The velocity profile, Eq. 30, correctly reduces to the form in the original MD-SF-PF model when the potential function becomes only a function of radial position [that is, $K_2(\rho)=K_3(\rho)$] and v_A is negligible. The profile in Eq. 30 also reduces to the Poiseuille parabolic velocity profile in the case of no potential function, free solution diffusivity, and pure solvent flow (that is, $\Phi(\rho,\xi)=0$, $b=1$, and $\pi_2=\pi_3=0$, respectively). The last term, LHS, effectively acts to distort the velocity profile from the parabolic shape as a result of the strong interactions between the solute and membrane. Ultimately, this leads to reduced flux with solute present, even for dilute solutions.

Solvent and solute flux through the membrane

The solvent and solute fluxes through a single pore are integrated over the area of the pore and then generalized for the fluxes over the surface area of the membrane as follows.

The average velocity of the solvent in a single pore is:

$$u_B=\frac{\int_0^1 u_B(\rho)\rho d\rho}{\int_0^1 \rho d\rho}=2\left(\frac{RT}{\tau\chi_{AB}}\right)\int_0^1 \alpha(\rho)\rho d\rho \quad (34)$$

and the average solvent flux is:

$$J_B=u_BC=2\left(\frac{CRT}{\tau\chi_{AB}}\right)\int_0^1 \alpha(\rho)\rho d\rho \quad (35)$$

Using Eq. 29, the average solute flux through the pore area is:

$$J_A=\frac{2}{\tau\chi_{AB}}\int_0^{1-\lambda}[\alpha(\rho)+\omega(\rho)]\left\{\pi_2+\frac{\pi_2-K^*(\rho)\pi_3}{e^{[\alpha(\rho)+\omega(\rho)]}-1}\right\}$$
$$\times\frac{e^{-\Phi(\rho,0)}}{b(\rho)}\rho d\rho \quad (36)$$

The above average fluxes for a single pore, J_A and J_B, are related to permeation fluxes through the membrane, N_A and N_B, using the fractional pore area,

$$N_B=\epsilon J_B \quad (37)$$

and

$$N_A=\epsilon J_A \quad (38)$$

Therefore, the total permeation flux through the membrane, N_T, is:

$$N_T=(N_A+N_B) \quad (39)$$

Material balance on the solute flux across the membrane,

$$C_{A3}=C\left(\frac{J_A}{J_A+J_B}\right)=C\left(\frac{N_A}{N_A+N_B}\right) \quad (40)$$

determines the permeate concentration.

The above analysis assumes that all the pores on the membrane surface have the same radius; the case of pore-size distribution is discussed elsewhere (Mehdizadeh and Dickson, 1989a).

Finally, the separation achieved by a membrane is determined from:

$$f'=\frac{C_{A2}-C_{A3}}{C_{A2}} \quad (41)$$

Potential and friction functions

In the original MD-SF-PF model, the following equation

describes the form of the potential function for the case of solute repulsion by membrane:

$$\Phi(\rho)=\begin{cases}\dfrac{\theta_1}{R_W}\,e^{1/2\rho^2} & \text{when } \rho<1-\lambda\\ \infty & \text{when } \rho\geq 1-\lambda\end{cases} \tag{42}$$

This equation still holds in the Extended MD-SF-PF model, for the case of dissociable solutes such as electrolytes, in which the potential function (and, therefore, the partition coefficient) is almost independent of feed concentration so that equal partition coefficients, on the two sides of the membrane, are expected (Lonsdale et al., 1967). However, strong solute-membrane affinity systems are usually associated with different partition coefficients on the two sides of a membrane (for example, Connell and Dickson, 1988). This implies that, in this case, the potential field depends on other factors such as solute concentration; likely due to both the strong solute-membrane attraction and solute-solute interactions. Anderson and Brannon (1981) and Post and Glandt (1985) have looked at the interesting problem of concentration dependent potential function (or equivalently partition coefficient) by looking at solute-solute interactions. Anderson and Brannon's work, as presented, leads to K values between 0 and 1 which would not explain the phenomena observed here. However, the approach taken by Post and Glandt could well describe the concentration dependent potential function needed in the current work. This possibility is left for future work; for now an empirical potential function, consistent with the data is used.

A first approximation to modeling of the concentration dependency may be as follows:

$$\Phi(\rho,\xi)=\frac{\theta_1}{R_W}\,e^{1/2\rho^2}f\{C_A(\rho,\xi)\} \tag{43}$$

where $f\{C_A(\rho,\xi)\}$ is some relationship between the potential function and the concentration inside the pore. However, whatever the $f\{C_A(\rho,\xi)\}$ should be, the concentration, $C_A(\rho,\xi)$, itself needs to be determined from the potential function (see Eq. 24). Therefore, the governing equations become highly coupled. In order to avoid such difficulty the $f\{C_A(\rho,\xi)\}$ term is separated into feed and permeate concentration and some axial dependency, in an empirical manner. One such correlation, which has been found in the present research to well represent the data (to be discussed in next section), is:

$$\Phi(\rho,\xi)=\begin{cases}\dfrac{\theta_1}{R_W}\,e^{1/2\rho^2}e^{\gamma\xi}\left[1+\dfrac{lnC_{A2}}{lnC_{A3}}\right] & \text{when } \rho<1-\lambda\\ \infty & \text{when } \rho\geq 1-\lambda\end{cases} \tag{44}$$

for dilute feed solutions (that is, $X_{A1}\ll 1.0$) of nondissociable organic solutes. In the above equation, θ_1 and γ are the two empirical parameters required to know the potential function. The separation of variables, from Eq. 43 to Eq. 44, decouples the problem and simplifies the solution of the model. The concentration dependency suggested in Eq. 44 implies that as the feed concentration of the uncharged organic solute is increased the potential function becomes less attractive, and, therefore, the separation should increase as expected (for example, Dickson, 1985). The γ parameter empirically models the axial variation of the potential inside the pore. The axial dependency in Eq. 44 suggests that as the solute molecules move through the pore they feel a stronger attraction potential, and the potential function at the pore end is, therefore, stronger than that in the pore inlet. This means that the partition coefficient at the pore exit is larger than the partition coefficient at the pore inlet, for the case of uncharged organic solutes, which means $K^*(\rho)>1$.

The friction parameter, $b(\rho)$, which is given by the Faxen equation in the MD-SF-PF model, is now allowed to vary in the radial direction inside the pore, in the Extended MD-SF-PF model. Originally, Matsuura and Sourirajan (1981) suggested an exponential radial dependency for $b(\rho)$ but later used an average b value. Satterfield et al. (1973), who have studied the problem of using an average b value, have found that the Faxen equation was not able to describe their experimental data for effective diffusivities of aromatic and paraffinic hydrocarbons in silica-alumina catalysts, and suggested an empirical correlation for the friction factor. Several other researchers have also found that the Faxen equation could not describe their experimental data (Anderson and Quinn, 1974; Deen et al., 1981). Anderson and Quinn (1974), who studied the problem of restricted diffusion in pores, agree with Bean (1972) that the radial dependence of $b(\rho)$ should be taken into account.

In the light of the above discussion, the Faxen equation might not be adequate for solute-membrane affinity case, and the following empirical modification, as suggested by Dickson (1985), is used in the Extended MD-SF-PF model:

$$b(\rho)=\begin{cases}b_{\text{Faxen}}\exp\left[\dfrac{E/R_W}{1-\rho}\right] & \text{when } \rho<1-\lambda\\ \infty & \text{when } \rho\geq 1-\lambda\end{cases} \tag{45}$$

where E is an adjustable parameter and b_{Faxen} is given by the Faxen equation,

$$b_{\text{Faxen}}=b(\rho)\Big|_{\rho=0}=(1-2.104\lambda+2.09\lambda^3-0.95\lambda^5)^{-1} \tag{46}$$

Equation 45 allows the friction function to vary markedly along the radial position inside the pore; the equation reduces to the Faxen equation when E becomes zero or far from the pore wall where the exponential term approaches 1.0 in large pores.

Equation 45 implies that when the parameter E is of the same (or larger) order of magnitude as (than) the pore size, R_W, very small diffusivities for the solute molecules are predicted. This is consistent with the mechanism that, due to the strong attraction potentials inside the pore, the solute molecules diffuse very slowly through the pore.

Results and Discussion

In this section, the results of simulations and model comparisons for the Extended MD-SF-PF model are presented. The model, as presented, is a four parameter model; that is the parameters R_W, θ_1, E, and γ must either be prespecified (for a simulation) or estimated based on experimental data (model comparison). A fifth parameter, τ/ϵ, is estimated from the pure water data. The experimental data, which have been

Table 1. Physicochemical Parameters for the Solutes Studied

	Toluene	Cumene	*p*-Cl-phenol
Partial molar volume,* $m^3/kmol$	0.106	0.140	0.112
Diffusivity,** $m^2/s, \times 10^9$	0.968	0.799	0.950
Solute Radius,† m, $\times 10^9$	0.252	0.305	0.256

*Estimated by the LeBas method or using pure solute density (pCl-phenol) (Reid et al., 1977)
**Estimated by method of Wilke-Chang (Reid et al., 1977).
†Hydrodynamic radius estimated by Stokes-Einstein Equation (Reid et al., 1977).

compared with the model predictions, are for aqueous solutions of toluene (Connell and Dickson, 1988), cumene (Dickson et al., 1983), and p-chlorophenol (Dickson et al., 1976). The values for the partial molar volumes (v_A), diffusivities (D_{AB}), and solute radii (R_A) are listed in Table I, along with method of estimation. The numerical method used to solve the nonlinear differential equation of the model, Eq. 30, is the orthogonal collocation method of weighted residuals as previously described (Mehdizadeh and Dickson, 1990).

Simulation results

To see how the model works under simulated conditions, the following operating conditions have been employed: $\Delta P = 1{,}000$ to 8,000 kPa, $T = 25°C$, $C_{A2} = 0.002925$ kmol/m^3 toluene in water, and a membrane with the following typical characteristics is assumed: $R_W = 24.0 \times 10^{-10}$ m, $\theta_1 = -54.0 \times 10^{-10}$ m, $E = 40.0 \times 10^{-10}$ m, $\gamma = 0.315$, and $\tau/\epsilon = 0.6686 \times 10^{-3}$ m. The membrane performance as predicted by the model is shown in Figure 3 in which the membrane separation, f', has been plotted vs. total permeation (volumetric) flux, J_v. As the system pressure is increased the separation decreases while the flux increases; this phenomenon is typical for solute-membrane affinity systems.

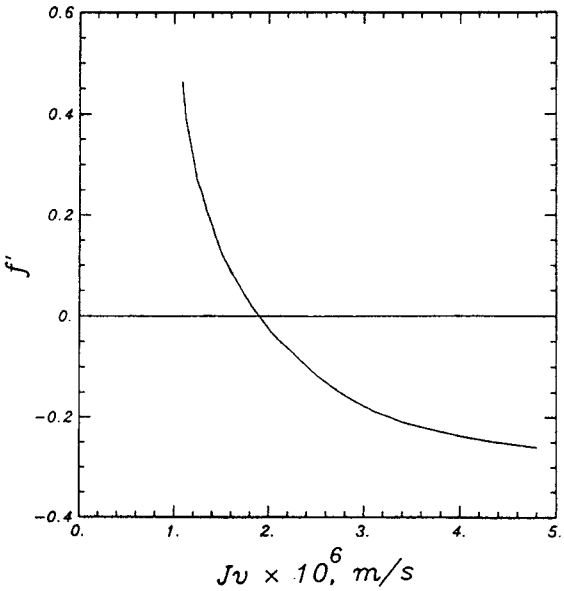

Figure 3. Separation vs. permeation flux for toluene water system simulated by the extended MD-SF-PF model at 25°C.

$C_{A2} = 0.002925$ kmol/m^3, $R_W = 24 \times 10^{-10}$ m, $\theta_1 = -54 \times 10^{-10}$ m, $E = 40 \times 10^{-10}$ m, $\gamma = 0.315$, and $\tau/\epsilon = 0.6686 \times 10^{-3}$ m.

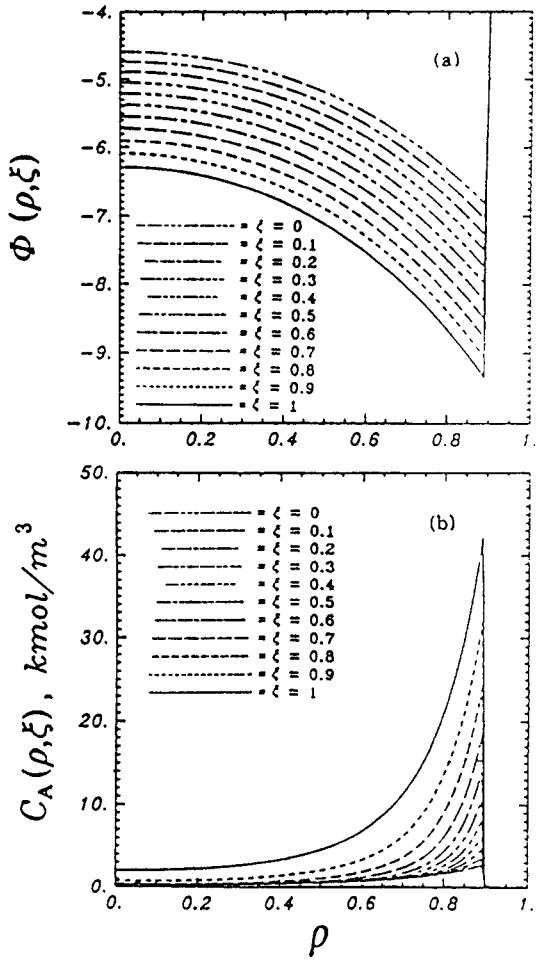

Figure 4. Simulation results for the data point in Figure 3 at 8,000 kPa.

(a) Potential function as a function of radial and axial positions inside the pore; (b) solute concentration as a function of radial and axial positions inside the pore.

Considering only one point on the curve of Figure 3, for example, at $\Delta P = 8{,}000$ kPa (corresponding to $f' = -0.26$ in Figure 3), the concentration profile inside the pore is presented in Figure 4, together with the potential function, as a function of radial and axial positions. Both the profiles, in Figure 4, have zero slopes at the pore centerline and have maximum slopes near the pore wall. The potential (negatives indicating the solute is attracted to the membrane) increases, in absolute value, from the inlet to the outlet of the pore; the concentration also increases in the same direction. Higher values of potential at the pore exit means higher values for the partition coefficient at the membrane exit compared with that at the membrane entrance; that is the partitioning effect is stronger at the pore exit.

In order to see how the Extended MD-SF-PF model behaves when feed concentration changes, simulation studies have been done for the system toluene-water with the following parameters for the membrane system: $R_W = 20 \times 10^{-10}$ m, $\theta_1 = -36 \times 10^{-10}$ m, $\gamma = 0.286$, $E = 40 \times 10^{-10}$ m, and $\tau/\epsilon =$

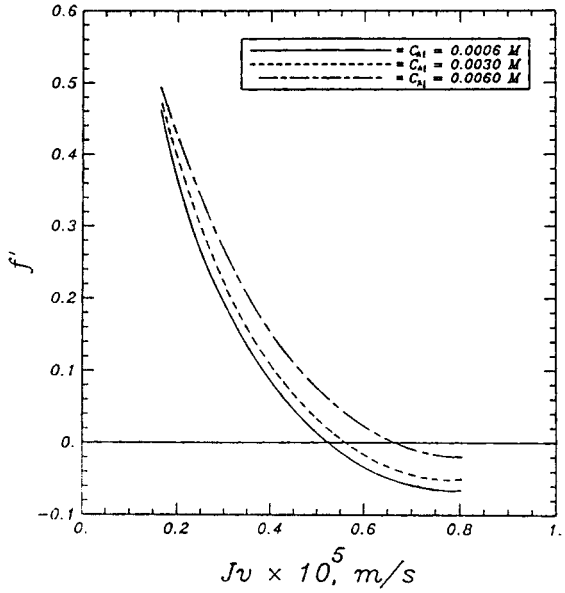

Figure 5. Theoretical separation vs. permeation flux, with feed concentration as a parameter, as simulated by the Extended MD-SF-PF model for toluene-water solution.

The membrane characteristics are: $R_W = 20 \times 10^{-10}$ m, $\theta_1 = -36 \times 10^{-10}$ m, $\gamma = 0.286$, $E = 40 \times 10^{-10}$ m, and $\tau/\epsilon = 0.4533 \times 10^{-3}$ m.

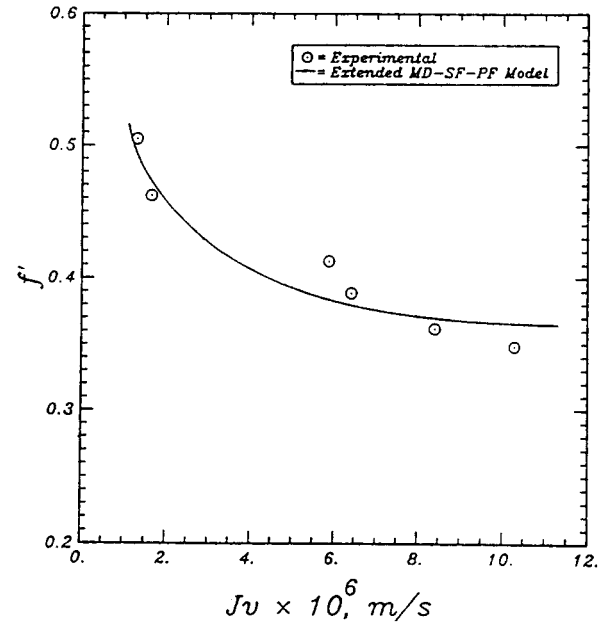

Figure 6. Experimental data vs. the extended MD-SF-PF model predictions for the toluene-water-cellulose acetate system at 25°C.

0.4533×10^{-3} m. The operating conditions are: $C_{A2} = 0.0006$ to 0.0060 kmol/m^3, $\Delta P = 2{,}000$ to 8,000 kPa; the system temperature remains constant at 25°C. The model behavior is depicted in Figure 5. For any feed concentration, the separation decreases as the pressure is increased, and as the feed concentration is increased the separation increases due to the weakening of the (negative) attraction potential field (see Eq. 44). The increase in separation, as the feed concentration is increased, can be seen in the literature (for example, Dickson et al., 1983; Connell and Dickson, 1988). The flux decline with increase in feed concentration is due to the concentration dependency of the potential function. The concentration dependent potential function means that the strength of the potential field, inside the membrane pores, depends on the number of solute molecules per unit volume of the pore, and the higher the concentration the weaker is the potential. That is, if the potential function can be represented by a Hamaker constant, for the case of nondissociable organics, the Hamaker constant changes as the solute concentration is changed.

Model comparison to data

The three systems which have been employed to test the extended MD-SF-PF model are dilute aqueous solutions of toluene (Connell and Dickson, 1988), cumene (Dickson et al., 1983), and p-chlorophenol (Dickson et al., 1976). The type of membrane used in all these cases was cellulose acetate. The Extended MD-SF-PF model was fitted to the experimental data of separation to determine the parameters of the model for each system; the procedure of parameter estimation has been discussed elsewhere (Mehdizadeh and Dickson, 1989c). The data sets available are small; too small to determine accurately four unknown parameters. Therefore, the purpose of the following data fitting is to show that the model can be consistent with data and correct trends are followed. No claim can be made as to the correctness of the model based on data fitting and the estimated parameters should not be compared. The results are as follows.

For the toluene-water-cellulose acetate system, the model fit to the data is illustrated in Figure 6 and the four unknown parameters are determined. Note that both the separation and the flux values are predicted by the model. In this case, the determined parameters are: $R_W = 23.16 \times 10^{-10}$ m, $\theta_1 = -32.33 \times 10^{-10}$ m, $E = 40.07 \times 10^{-10}$ m, and $\gamma = 0.2858$. The value of τ/ϵ has been estimated from pure water experiments as 0.4533×10^{-3} m using the method in Mehdizadeh and Dickson (1991). The model fits the data well; as the permeation flux is increased (by increasing the system pressure) the separation decreases. The separation decreases with an increase in pressure because, at higher pressures, the mobility of the solute molecules is increased in the membrane pores due to the higher convective forces, against the membrane-solute attraction force. The feed concentrations in this case are in the range of 0.0004 to 0.004 kmol/m^3, and the operating pressures are in the range of 1,000 to 7,000 kPa. The temperature in all these systems remains constant at 25°C.

There are two main reasons for the discrepancy between the model and the data points in Figure 6. Firstly, there is some error in the measurement of both the volume flux, J_v, and the theoretical separation, f', which is calculated dependent on the mass-transfer coefficient which is also subject to experimental error. Secondly, the data points were measured at different feed concentrations of toluene, and as illustrated in Figure 5, concentration has a significant effect on flux and separation. The unknown parameters were assumed concentration independent, during estimation, and the line shown is a smooth curve drawn through the model estimates.

For the cumene-water-cellulose acetate system, the results

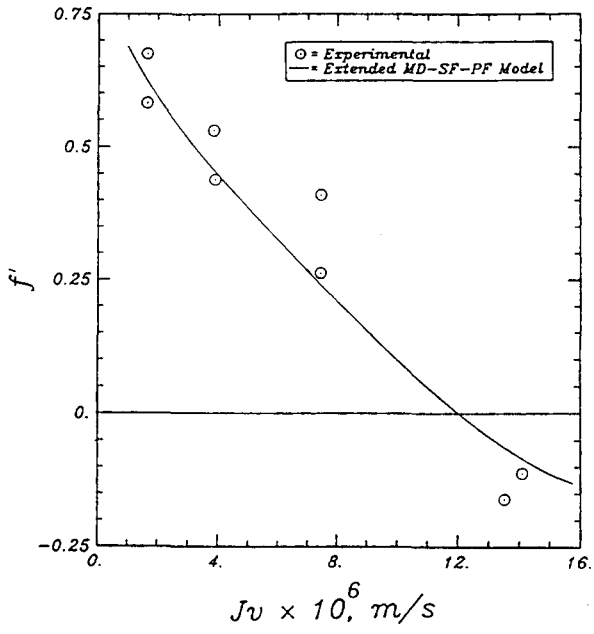

Figure 7. Experimental data vs. the extended MD-SF-PF model predictions for the cumene-water-cellulose acetate system at 25°C.

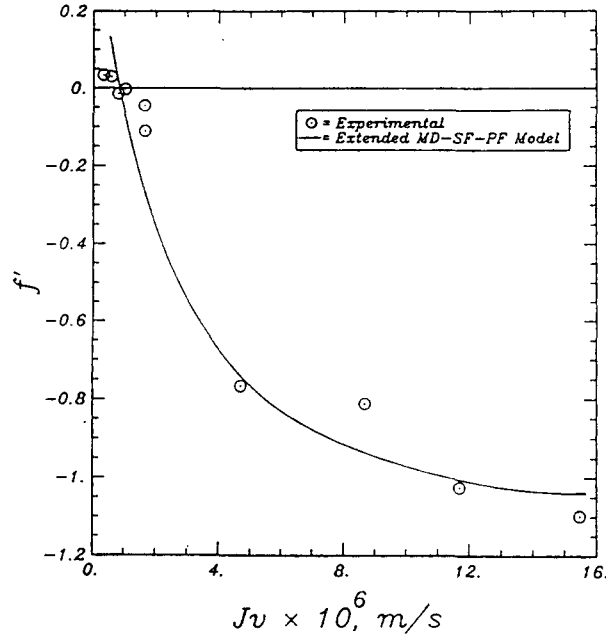

Figure 8. Experimental data vs. the extended MD-SF-PF model predictions for the p-chlorophenol-water-cellulose acetate system at 25°C.

are shown in Figure 7. The feed concentrations are in the range of 60.0×10^{-6} to 200×10^{-6} kmol/m^3, and the operating pressures are in the range of 690 to 6,900 kPa. The system temperature remains at 25°C. The model parameters determined from the data fitting are: $R_W=11.98\times10^{-10}$ m, $\theta_1=-36.23\times10^{-10}$ m, $E=41.79\times10^{-10}$ m, and $\gamma=0.1809$. The value of τ/ϵ has been determined from pure water experimental data as 0.8755×10^{-4} m. The model, as represented by the curve in Figure 7, is trying to best represent the experimental data which has a large scattering. For this system, as for the toluene-water system, there are deviations due to experimental errors and due to different feed concentrations in the data. The model can well describe the performance of the membrane when the separation decreases from positive to negative values. In this case, the separation attains values as low as -15%.

The model description of data for the case of p-chlorophenol-water-cellulose acetate system is shown in Figure 8. The feed concentrations are in the range of 0.0001 to 0.004 kmol/m^3, and the operating pressures are in the range of 690 to 10,350 kPa. The system temperature remains at 25°C. The model parameters determined from the data fitting are: $R_W=17.38\times10^{-10}$ m, $\theta_1=-40.13\times10^{-10}$ m, $E=42.28\times10^{-10}$ m, and $\gamma=0.0407$. The value of τ/ϵ has been determined from pure water experimental data as 0.3519×10^{-3} m. Again, there are deviations due to experimental errors and due to different feed concentrations in the data. The model description of the experimental data is successful as the separation decreases from about 10% down to about -100%. The large negative separations, such as -100%, imply that the solute molecules have faced a strong (adsorption) potential field inside the membrane pores.

The values of E (representing the frictional drag in Eq. 45) and R_W, in all the cases discussed above, are such that the friction function, $b(\rho)$, has values that are much larger than those predicted by the Faxen equation. Therefore, the Extended MD-SF-PF model implies that once the organic solute molecules are sorbed by the membrane the frictional drag on the solute molecules can be large so that the molecules move slowly through the membrane pores.

Overall, the Extended MD-SF-PF model has been able to describe the experimental data for the three systems of toluene-water ($f'=50\%$ to 37%), cumene-water ($f'=65\%$ to -15%), and p-chlorophenol ($f'=10\%$ to -100%), with cellulose acetate membranes. The separation values for the above three organic solutes is in the order of toluene > cumene > p-chlorophenol (that is, p-chlorophenol yields the poorest separation values). The p-chlorophenol and other phenol derivatives are of practical interest in wastewater treatment. The negative separation for p-chlorophenol implies that the solute would be enriched in the permeate with cellulose acetate membrane material; worse than no separation at all.

The reason for the negative separation of p-chlorophenol (that is, preferential sorption of the solute) might be as follows. The membrane material (that is, cellulose acetate) has a net proton acceptor character due to a slightly negatively charged. Since p-chlorophenol has a higher acidity than water (Matsuura and Sourirajan, 1971), *p*-chlorophenol should be more attracted to the membrane surface than water. Therefore, p-chlorophenol is preferentially sorbed at the membrane-solution interface. On the other hand, *p*-chlorophenol has less mobility than water, and the solute mobility tends to increase with increase in operating pressure (Dickson et al., 1979). The increased mobility of the solute molecules with pressure is due to the increased shear effect on the solute molecules by the increased fluid velocity. The facts that p-chlorophenol is preferentially sorbed to the membrane and the solute mobility, in the membrane, increases with pressure are well predicted by the Extended MD-SF-PF model. The overall concentration profile for such a system was shown in Figure 1b.

For the toluene-water system, the solute molecules are still attracted to the membrane by the attractive potential forces; however, positive separations are obtained due to the smaller mobility of the solute molecules, as compared with the p-chlorophenol molecules. The overall concentration profile for such a system was shown in Figure 1a.

Conclusions

This article extends the modified surface force-pore flow transport model of reverse osmosis in several ways and, as a result, an extended model (called the Extended MD-SF-PF model) is obtained which is able to describe the complicated behavior of strong solute-membrane affinity systems in reverse osmosis. It has been shown that the peculiar case of solute-membrane affinity is mainly due to the partition coefficient effect at the membrane-solution interfaces (which is, in turn, controlled by the potential field inside the membrane), but once the solute molecules are sorbed into the membrane they can attain different mobilities inside the membrane pores depending on the net force upon them. The model has been tested against three different (dilute) aqueous solutions of toluene, cumene, and p-chlorophenol with cellulose acetate membranes. The model seems very promising to describe these systems.

Acknowledgments

The authors wish to acknowledge the financial assistance of the Natural Sciences and Engineering Research Council of Canada (NSERC) and the useful scientific and editorial suggestions made by the reviewers of this article.

Notation

a_A = activity of solute, dimensionless
$b(\rho)$ = friction parameter defined by Eq. 14, dimensionless
C = molar density of solution, kmol/m^3
$C_A(r, z)$ = solute concentration inside a pore at position r and z, kmol/m^3
$C_A(\rho, \xi)$ = solute concentration inside a pore at dimensionless position ρ and ξ, kmol/m^3
D_{AB} = solute diffusivity in free solution, m^2/s
D_{AM} = solute diffusivity inside a pore, m^2/s
E = friction parameter in Eq. 45, m
f' = theoretical separation defined by Eq. 41, dimensionless
F_A = total force driving solute through a pore, kJ/m·kmol
F_{AB} = frictional force between solute and solvent, kJ/m·kmol
F_{AM} = frictional force between solute and pore wall, kJ/m·kmol
J_A = vector of solute flux through a single pore, kmol/m^2·s
$J_{A,r}$ = radial component of solute flux through a single pore, kmol/m^2·s
$J_{A,z}(r)$ = axial component of solute flux through a single pore, kmol/m^2·s
J_A = radially averaged solute flux through a single pore, kmol/m^2·s
J_B = radially averaged solvent flux through a single pore, kmol/m^2·s
J_v = volumetric flux in a membrane, m^3/m^2·s
k_0 = Boltzmann's constant, kJ/K
$K^*(\rho)$ = parameter defined by Eq. 25, dimensionless
$K_i(\rho)$ = partition coefficient at position i, defined by Eqs. 4 and 5, dimensionless
N_i = flux of i through membrane, kmol/m^2·s
P = hydrostatic pressure, kPa
r = cylindrical coordinate normal to the pore wall, m
R = gas constant, kJ/kmol·K
R_i = average radius of i, m
T = temperature, K
$u_A(r, z)$ = solute velocity inside a pore, m/s
$u_B(r)$ = solvent velocity inside a pore, m/s
v_A = partial molal volume of solute, m^3/kmol
z = cylindrical coordinate parallel to the pore wall, m

Greek letters

α = velocity defined by Eq. 15, dimensionless
β_1 = parameter defined by Eq. 31, dimensionless
γ = potential parameter in Eq. 44, dimensionless
ΔP = pressure drop across the membrane, kPa
ϵ = fractional pore area of membrane, dimensionless
η = solution viscosity, kPa·s
θ_1 = potential parameter in Eqs. 42 and 44, m
λ = ratio of solute molecular radius to pore radius, dimensionless
μ_A = total potential of solute, kJ/kmol
μ_A^o = total potential of solute at standard state, kJ/kmol
ξ = axial coordinate defined by z/τ, dimensionless
$\pi(\rho, \xi)$ = osmotic pressure inside the pore, kPa
π_i = osmotic pressure of solution at position i, kPa
ρ = radial coordinate defined by r/R_W, dimensionless
σ_i = Staverman coefficient at position i, dimensionless
τ = average pore length taking tortuosity into account, m
τ_{rz} = cylindrical-coordinate shear stress, kPa
ϕ = potential function, kJ/kmol
Φ = potential function defined by Eq. 4 and 5, dimensionless
χ_{ij} = frictional constant between i and j, kJ·s/m^2·kmol
$\omega(\rho)$ = parameter defined by Eq. 26, dimensionless

Subscripts

A = solute
B = solvent
M = membrane
T = total solution
W = pore wall
1 = feed solution
2 = boundary-layer solution
3 = permeate solution

Literature Cited

Anderson, J. E., S. J. Hoffman, and C. R. Peters, "Factors Influencing Reverse Osmosis Rejection of Organic Solutes from Aqueous Solutions," *J. Phys. Chem.*, **76**, 4006 (1972).

Anderson, J. L., and J. H. Brannon, "Concentration Dependence of the Distribution Coefficient for Macromolecules in Porous Media," *J. Polym. Sci.*, **19**, 405 (1981).

Anderson, J. L., and D. M. Malone, "Mechanism of Osmotic Flow in Porous Membranes," *Biophys. J.*, **14**, 957 (1974).

Anderson, J. L., and J. A. Quinn, "Restricted Transport in Small Pores: A Model for Steric Exclusion and Hindered Particle Motion," *Biophys. J.*, **14**, 130 (1974).

Bean, C. P., "The Physics of Porous Membranes: Neutral Pores," in: *Membranes: A Series of Advances*, G. Eisenmen, ed., Vol. 1, Marcel-Dekker, New York (1972).

Burghoff, H.-G., K. L. Lee, and W. Pusch, "Characterization of Transport Across Cellulose Acetate Membranes in the Presence of Strong Solute-Membrane Interactions," *J. Appl. Polym. Sci.*, **25**, 323 (1980).

Connell, P. J., and J. M. Dickson, "Modeling of Reverse Osmosis Separations with Strong Solute-Membrane Affinity at Different Temperatures Using the Finely Porous Model," *J. Appl. Polym. Sci.*, **35**(5), 1129 (1988).

Deen, W. M., M. P. Bohrer, and N. B. Epstein, "Effects of Molecular Size and Configuration on Diffusion in Microporous Membranes," *AIChE J.*, **27**, 952 (1981).

Dickson, J. M., "Reverse Osmosis in the Presence of Strong Solute-Membrane Affinity," PhD Thesis, Virginia Polytechnic Institute and State University (1985).

Dickson, J. M., T. Matsuura, and S. Sourirajan, Unpublished data (1976).

Dickson, J. M., T. Matsuura, and S. Sourirajan, "Transport Char-

acteristics in the Reverse Osmosis System p-Chlorophenol-Water-Cellulose Acetate Membrane," *Ind. Eng. Chem. Process Des. Dev.*, **18**, 641 (1979).
Dickson, J. M., M. Babai-Pirouz, and D. R. Lloyd, "Aromatic Hydrocarbon-Water Separations by a Pressure-Driven Membrane Separation Process," *Ind. Eng. Chem. Process Des. Dev.*, **22**, 625 (1983).
Higuichi, A., and T. Nakagawa, "Membrane Potential and Ion Transport in Inhomogeneous Ion-exchange Membranes," *J. Chem. Soc.*, Faraday Trans., **85**, 3609 (1989).
Jacazio, G., R. F. Probstein, A. A. Sonin, and D. Yung, "Electrokinetic Salt Rejection in Hyperfiltration through Porous Materials. Theory and Experiment," *J. Phys. Chem.*, **76**, 4015 (1972).
Jonsson, G., "Methods for Determining the Selectivity for Reverse Osmosis Membranes," *Desalination*, **24**, 19 (1978).
Jonsson, G., and C. E. Boesen, "Water and Solute Transport Through Cellulose Acetate Reverse Osmosis Membranes," *Trans. Faraday Soc.*, **17**, 145 (1975).
Lloyd, D. R., M. Babai-Pirouz, and J. M. Dickson, "Cyclic Hydrocarbon-Water Separation using a Pressure-Driven Membrane Separation Process," *J. Separ. Technol.*, **3**(4), 21 (1982).
Lonsdale, H. K., U. Merten, and M. Tagami, "Phenol Transport in Cellulose Acetate Membranes," *J. Appl. Polym. Sci.*, **11**, 1807 (1967).
Matsuura, T., and S. Sourirajan, "Physicochemical Criteria for Reverse Osmosis Separation of Alcohols, Phenols, and Monocarboxylic Acids in Aqueous Solutions Using Porous Cellulose Acetate Membranes," *J. Appl. Polym. Sci.*, **15**, 2905 (1971).
Matsuura, T., and S. Sourirajan, "Physicochemical Criteria for Reverse Osmosis Separation of Monohydric and Polyhydric Alcohols in Aqueous Solutions Using Porous Cellulose Acetate Membranes," *J. Appl. Polym. Sci.*, **17**, 1043 (1973a).
Matsuura, T., and S. Sourirajan, "Reverse Osmosis Separation of Hydrocarbons in Aqueous Solutions Using Porous Cellulose Acetate Membranes," *J. Appl. Polym. Sci.*, **17**, 3683 (1973b).
Matsuura, T., P. Blais, J. M. Dickson, and S. Sourirajan, "Reverse Osmosis Separations for Some Alcohols and Phenols in Aqueous Solutions Using Aromatic Polyamide Membranes," *J. Appl. Polym. Sci.*, **18**, 3671 (1974).
Matsuura, T., and S. Sourirajan, "Reverse Osmosis Transport Through Capillary Pores Under the Influence of Surface Forces," *Ind. Eng. Chem. Proc. Des. Dev.*, **20**, 273 (1981).
Mehdizadeh, H., "Modeling of Transport Phenomena in Reverse Osmosis Membranes," PhD Thesis, McMaster University, Ontario, Canada (1990).
Mehdizadeh, H., and J. M. Dickson, "Theoretical Modification of the Surface Force-Pore Flow Model for Reverse Osmosis Transport," *J. Memb. Sci.*, **42**, 119 (1989a).
Mehdizadeh, H., and J. M. Dickson, "The Role of Surface Potential Functions in Determining Reverse Osmosis Transport Phenomena," *Proc. 2nd Int. Conf. Sep. Sci. Tech.*, Hamilton, Ontario, Canada, Oct. 1-4 (1989b).
Mehdizadeh, H., and J. M. Dickson, "Solving Nonlinear Differential Equations of Membrane Transport Models by Orthogonal Collocation," *Computers Chem. Eng.*, **14**(2), 157 (1990).
Mehdizadeh, H., and J. M. Dickson, "Evaluation of Surface Force-Pore Flow and Modified Surface Force-Pore Flow Models for Reverse Osmosis Transport," *Chem. Eng. Commun.*, **103**, 65 (1991).
Merten, U. (ed.), *Desalination by Reverse Osmosis*, MIT Press, MA, p. 15 (1966).
Post, A. J., and E. D. Glandt, "Equilibrium Partitioning in Pores with Adsorbing Walls," *J. Colloid Int. Sci.*, **108**, 31 (1985).
Reid, R. C., J. M. Prausnitz, and T. K. Sherwood, *The Properties of Gases and Liquids*, 3rd ed., McGraw-Hill, New York (1977).
Satterfield, C. N., C. K. Colton, and W. H. Pitcher, Jr., "Restricted Diffusion in Liquids Within Fine Pores," *AIChE J.*, **19**, 628 (1973).
Spiegler, K. S., "Transport Processes in Ionic Membranes," *Trans. Farad. Soc.*, **54**, 1408 (1958).
Thiel, S. W., D. R. Lloyd, and J. M. Dickson, "Analysis of Transport in a Pressure-Driven Membrane Separation Process," in "Reverse Osmosis and Ultrafiltration," S. Sourirajan and T. Matsuura, eds., Chap. 9, *ACS Symposium Series 281*, Washington, D.C. (1985a).
Thiel, S. W., D. R. Lloyd, and J. M. Dickson, "Physicochemical Interpretation of the Behavior of a Pressure-Driven Membrane Separation Process," in "Reverse Osmosis and Ultrafiltration," S. Sourirajan and T. Matsuura, eds., Chap. 10, *ACS Symposium Series 281*, Washington, D.C. (1985b).

Appendix I: Force Balance on the Solute in a Pore

The force balance on the solute inside a pore is (Mehdizadeh and Dickson, 1989a):

$$F_A(r,z) = -\{F_{AB}(r,z) + F_{AM}(r,z)\} \tag{AI.1}$$

where $F_A(r,z)$ is the total force driving the solute through the pore, and $F_{AB}(r,z)$ and $F_{AM}(r,z)$ are the frictional force between the solute and solvent and between the solute and the pore wall, respectively. $F_{AM}(r,z)$ is given by the definition of friction constant between the solute and the pore wall (Mehdizadeh and Dickson, 1989a):

$$F_{AM}(r,z) = -\chi_{AM}(r)[u_A(r,z) - 0] = -\chi_{AM}\frac{J_{A,z}(r)}{C_A(r,z)} \tag{AI.2}$$

Then, combining Eqs. AI.1, AI.2, and 11 gives:

$$-F_{AB}(r,z) = -\frac{RT}{\pi(r,z)}\frac{\partial\pi(r,z)}{\partial z} - v_A\frac{\partial P(r,z)}{\partial z} - \chi_{AM}J_{A,z}(r)\frac{RT}{\pi(r,z)} \tag{AI.3}$$

On the other hand,

$$u_A(r,z) = \frac{J_{A,z}(r)}{C_A(r,z)} \tag{AI.4}$$

and, by definition (Spiegler, 1958),

$$F_{AB}(r,z) = -\chi_{AB}[u_A(r,z) - u_B(r)] \tag{AI.5}$$

so that, using van't Hoff's theorem, Eqs. AI.4 and AI.5 are combined as:

$$J_{A,z}(r) = \frac{1}{\chi_{AB}}\frac{\pi(r,z)}{RT}[-F_{AB}(r,z)] + \frac{\pi(r,z)u_B(r)}{RT} \tag{AI.6}$$

Then, using Eq. AI.3 and $D_{AB} = RT/\chi_{AB}$ (Spiegler, 1958), and converting to dimensionless position, Eq. AI.6 can be written as:

$$J_{A,z}(\rho) = \frac{1}{\tau\chi_{AB}b(\rho)}\left\{-\frac{\partial\pi(\rho,\xi)}{\partial\xi} - v_A\frac{\pi(\rho,\xi)}{RT}\frac{\partial P(\rho,\xi)}{\partial\xi} + \alpha(\rho)\pi(\rho,\xi)\right\} \tag{AI.7}$$

where $\alpha(\rho)$ is the dimensionless solution velocity defined by Eq. 15.

From Eq. 23 the axial gradient of osmotic pressure is:

$$\frac{\partial\pi(\rho,\xi)}{\partial\xi} = -[\pi_2 - K^*(\rho)\pi_3] \times [\alpha(\rho) + \omega(\rho)]\frac{e^{[\alpha(\rho)+\omega(\rho)]\xi}}{e^{[\alpha(\rho)+\omega(\rho)]} - 1}e^{-\Phi(\rho,0)} \tag{AI.8}$$

which is used to find the axial component of solute flux as Eq. 29.

Appendix II: Derivation of Velocity Profile

The force balance on the elemental fluid of Figure 2 consists of the following three parts:

(1) The net force due to difference in pressure,

$$(2\pi r dr)\left\{(P|_z - \left[(P|_z + \left(\frac{\partial P}{\partial z}\right|_z dz\right]\right\} = -2\pi r dr dz \frac{\partial P(r,z)}{\partial z} \quad \text{(AII.1)}$$

(2) The net force due to viscous shear stresses, using Newton's law of viscosity,

$$(2\pi r dz)\left\{(\tau_{rz}|_z - (\tau_{rz}|_{r+dr}\right\} = \eta\left\{(2\pi r dr dz)\frac{d^2u_B(r)}{dr^2} + (2\pi dr dz)\frac{du_B(r)}{dr}\right\} \quad \text{(AII.2)}$$

(3) The net force due to the friction force between solute and the pore wall,

$$F_{AM}(2\pi r dr dz)C_A(r,z) = [-\chi_{AM}(r)u_A(r,z)](2\pi r dr dz)C_A(r,z) = -(2\pi r dr dz)\chi_{AM}(r)J_{A,z}(r) \quad \text{(AII.3)}$$

where $\chi_{AM}(r)$ is defined in Eq. AI.2. Substituting for $J_{A,z}(\rho)$ from Eq. 29 and substituting for dimensionless axial and radial positions, Eq. AII.3 becomes:

$$F_{AM}(\rho,\xi)(2\pi\rho d\rho d\xi)C_A(\rho,\xi) = -(2\pi\rho d\rho d\xi)\chi_{AM}(\rho)\left[\frac{\alpha(\rho)+\omega(\rho)}{\tau\chi_{AB}b(\rho)}\right] \times \left\{\pi_2 + \frac{\pi_2 - K^*(\rho)\pi_3}{e^{[\alpha(\rho)+\omega(\rho)]}-1}\right\}e^{-\Phi(\rho,0)} \quad \text{(AII.4)}$$

Adding up all the three contributions of the force balance and substituting for dimensionless axial and radial position, the differential equation for the solution velocity profile is derived as given by Eq. 30.

Manuscript received July 15, 1991, and revision received Aug. 28, 1992.